Nonlinear Elongation Flows in Associating Polymer Melts: From Homogeneous to Heterogeneous Flow

Supun S. Mohottalalage,[1] Manjula Senanayake,[1] Joel T. Clemmer,[2] Dvora Perahia,[1] Gary S. Grest,[2] and Thomas O'Connor[2,3]

[1]*Department of Chemistry, Clemson University, Clemson, South Carolina 29634, USA*
[2]*Sandia National Laboratories, Albuquerque, New Mexico 87185, USA*
[3]*Department of Materials Science and Engineering, Carnegie Mellon University, Pittsburgh, Pennsylvania 15213, USA*

(Received 14 October 2021; revised 16 December 2021; accepted 7 March 2022; published 28 April 2022)

Response to elongational flow is fundamental to soft matter and directly impacts new developments in a broad range of technologies form polymer processing and microfluidics to controlled flow in biosystems. Of particular significance are the effects of elongational flow on self-assembled systems where the interactions between the fundamental building blocks control their adaptation. Here we probe the effects of associating groups on the structure and dynamics of linear polymer melts in uniaxial elongation using molecular dynamics simulations. We study model polymers with randomly incorporated backbone associations with interaction strengths varying from $1k_BT$ to $10k_BT$. These associating groups drive the formation of clusters in equilibrium with an average size that increases with interaction strength. Flow drives these clusters to continuously break and reform as chains stretch. These flow-driven cluster dynamics drive a qualitative transition in polymer elongation dynamics from homogeneous to nanoscale localized yield and cavitation as the association strength increases.

DOI: 10.1103/PhysRevX.12.021024

Subject Areas: Computational Physics
Materials Science, Soft Matter

Response to elongational forces is fundamental to what makes soft matter soft, and it encapsulates a broad range of phenomena. Dense complex fluids, from slurries and colloids to blood flow, and industrially processed polymers, either form or function under elongational flow [1–3]. The shape, the dimensions, and the adaptability of the building blocks of these complex fluids determine their structure and dynamics during elongation. Polymer melts are one such dense system with immense technological significance [4–6] that are routinely processed under elongational flow. Many of these macromolecules contain associating groups that are critical for their technological function and at the same time drive unique rheological behavior. While the challenges in processing of associative polymers have been long realized [7–11], little is known about the response of these complex fluids to uniaxial elongational flow. Here, using molecular dynamics simulations, we show that the heterogeneous breakup of the associative clusters under flow drive dynamic heterogeneity of chains and create nanostructured flow patterns that significantly alter the processing of these complex fluids. Under strong flow the associative clusters rapidly break up and reform. We show that at the highest flow rates, the cluster-size distribution becomes independent of the strength of the associating groups as the flow becomes so strong that it overpowers the associative interactions, resulting in a convergence of the terminal viscosity at high flow rate.

Formation of associative polymer complexes is driven by a variety of molecular interactions including hydrogen bonding, π-π interactions, metal-ligand coordination, and long-lived ionic interactions [12,13]. These mechanisms can differ substantially in the coordination and cohesive strength of their associations. Hydrogen bonding and π-π interactions are governed by short-range interactions with strengths of association that depend on the polarizability and steric interactions of the associating groups. In contrast, ionizable associating groups exhibit long-range forces and thus result in large clusters with complex nanostructures that control the structure, dynamics, and rheological response of ionic polymers [14]. However, the impact of the interaction strength of the associating groups influences the structure of the clusters under elongational flow and their resulting impact on the overall flow response remains unknown.

The technological impact of elongational flow on complex fluids formed by polymers has motivated a number of

experimental and computational studies. For nonassociating systems, several recent experimental efforts have probed the structure and rheology of entangled [10,11,15,16] and unentangled [16–18] homopolymer melts and solutions in extensional flows where the degree of entanglement controls their viscoelastic response. These studies have observed that strong extensional flows significantly elongate polymer chains as expected, but generate distinct trends in nonlinear viscosities that vary with elongation rate, molecular weight N, entanglement segment length N_e [19,20], dilution ϕ [21,22], and proximity to the glass transition temperature T_g [23].

Molecular dynamics simulations have been able to relate some of these trends in nonlinear rheology to changes in viscous dissipation as chains become highly elongated in melts and solutions [24–27]. O'Connor and co-workers [24,25] recently showed that the rate dependence of the extensional viscosity of homopolymer melts changes with molecular weight N due to a crossover in dissipation mechanism as elongation rates increase. At low rates, the dissipation is dominated by diffusive relaxation of chain conformations, whereas at high rates the dissipation is dominated by the advective drag of the flow field on the elongated chains. Polymer solutions also exhibit a sharp distinction between their *equilibrium* modes of dissipation and their *nonequilibrium* dissipation in elongated states. Recent theoretical models were successful in predicting the rate-dependent viscosity of elongated systems observed in experiments. These models promote tube model parameters like the monomeric friction and entanglement density to dynamic variables that can evolve as functions of the nonequilibrium chain order [26,28–31].

Less is known for associating systems in nonlinear elongation. For ionic polymers, Shabbir and co-workers [15,16] and Wu *et al.* [18] reported that increasing the strength of the associating groups increases the elastic modulus and decreases processability. These authors showed that extension rates faster than the reciprocal of the associating group lifetime lead to brittle failure and extension rates slower than the reciprocal of the associating group lifetime lead to continuous stretching that nearly reaches steady state at the highest Hencky strain ~5. Hinton and co-workers [10,11] demonstrated that weakening the strength of the association from that of ionic interactions to hydrogen bonding further decreased the elastic modulus and only moderately increases processability. Recently, Schaefer *et al.* [32] developed theories that predict that the intermolecular reversible cross-links in silk proteins can shift the alignment-to-stretch transition of semidilute polymers to much smaller strain rates. Schaefer and McLeish [33] also found that intermolecular associations in silk can also reduce the critical specific work for flow-induced crystallization.

Here we employ molecular simulations to study the structural evolution and rheological behavior of associating

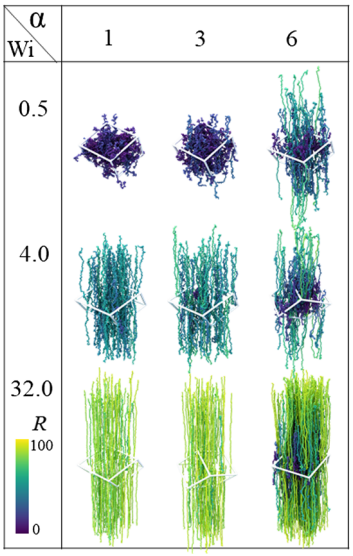

FIG. 1. Snapshots illustrating chain stretching for associating group strength $\alpha = 1$, 3, and 6 for Wi = 0.5, 4, and 32 at strain $\varepsilon = 10$. For clarity, 1/4 of systems are shown. Chains are colored according to their end-to-end distance R.

polymer melts under elongation flow. The complexity of the system is reduced by using a coarse-grained bead-spring model in which the association groups are incorporated in the form of beads with stronger cohesive attraction. These "sticky beads" are randomly distributed along the chain backbone [34]. The strength of the interaction between associating groups is varied from $1k_BT$ to $10k_BT$. The lower end of this range is characteristic of the interaction energies that drive copolymer assembly. With increasing interaction strength, the model captures the association of polar groups, such as those present in nonionic surfactants, and our largest interactions approach ionic interaction strengths. This range is sufficient to produce qualitative changes in both the equilibrium cluster structure and nonlinear flow behavior of our associating melts, as illustrated in Fig. 1.

Polymers are modeled with a fully flexible bead-spring model [35]. A homopolymer melt with no associating groups of 500 linear chains of length $N = 100$ beads of mass m and diameter σ were first constructed following the procedure of Auhl *et al.* [36]. The beads are connected with finitely extensible springs. The beads interact with a Lennard-Jones (LJ) potential with a length scale σ, cutoff $r_{\text{cut}} = 2.5\sigma$, and energy scale $\varepsilon_{\alpha\beta}$. The indices $\alpha\beta$ are either 1 or 2 and indicate bead type. We include associativity by using two types of beads. Nonassociating beads are type 1 and interact with a LJ cohesion strength ε_{11}. After the homopolymer melt is equilibrated, we randomly select five beads on each chain to be associating beads of type 2. The cohesion between associating groups is modeled by setting the LJ interaction strength $\varepsilon_{22} \geq \varepsilon_{11}$. The cross term is set to $\varepsilon_{12} = \varepsilon_{11}$ so that only pairs of associating beads experience

excess cohesion. Each system is then run for $10^7\tau$, where $\tau = \sigma\,(m/\varepsilon_{11})^{1/2}$, until the average cluster size of the associating groups no longer changes [34]. All simulated melts are maintained at a temperature $T = \varepsilon_{11}/k_B$, which is $\sim 2T_g$ [37] and we vary the dimensionless ratio $\alpha = \varepsilon_{22}/\varepsilon_{11}$ from 1 to 10 such that interaction energy between associating beads ranges from $1k_BT$ to $10k_BT$.

The equations of motion are integrated with a time step $\Delta t = 0.01\tau$ at temperature $T = \varepsilon_{11}/k_B$ with a thermostat damping time of 10τ and density $\rho \approx 0.89\sigma^{-3}$. To model uniaxial extensional flow, melts are elongated along the z axis of the simulation box at a constant Hencky strain rate $\dot{\varepsilon} \equiv \partial\Lambda/\partial t$, where Λ is the stretch ratio along the z axis. Since polymers are nearly incompressible, the two perpendicular directions both contract as $\Lambda^{-1/2}$. Flow is maintained by integrating the g-SLLOD equations of motion [38] with a Nosé-Hoover thermostat. The simulation box is regularly remapped during flow with generalized Kraynik-Reinelt boundary conditions to prevent the simulation cell from becoming too skewed [39,40]. During flow, we measure the extensional stress $\sigma_E = \sigma_{zz} - 0.5(\sigma_{xx} + \sigma_{yy})$ and the transient extensional viscosity (stress-growth coefficient) $\eta_E^+(\varepsilon) = \sigma_E/\dot{\varepsilon}$.

Unlike experiments, simulations with periodic boundary conditions can maintain uniaxial elongation flows of bulk fluids to arbitrarily large strains. This allows us to maintain flows well past experimental limits and accumulate sufficient statistics to resolve distributions for cluster sizes and chain conformations over large strains. The stress reaches a time-independent plateau after a true strain of $\varepsilon = 4$, as shown in Fig. 2(a). The results reported here are obtained by averaging simulation data over a strain interval $\varepsilon = 5$–10, which we refer to as steady state. In this regime all measured quantities such as the average end-to-end distance $\langle R \rangle$ of the chains and cluster distribution do not change. Over this range of strain, the stress fluctuates (due to finite size effects) about a well-defined average value. In this regime we denote the average steady-state viscosity by η_E to distinguish from the early time transient viscosity $\eta_E^+(\varepsilon)$. We note that this interval is given in true strain such that the range of $\varepsilon = 5$–10 corresponds to stretch ratios λ from ~150 to 22 000. This interval, enabled by periodic simulations, is much larger than can be assessed by experiments and thus provides the first microscopic insight into the steady-state extensional flow of associating polymers.

The strength of flow is measured in terms of a dimensionless Weissenberg number $\mathrm{Wi} = \dot{\varepsilon}\tau_R$, where $\tau_R = \tau_e Z^2$ is the Rouse time [41] for chains in a melt with no associating groups ($\alpha = 1$). The Rouse time is the longest dissipative relaxation time for a linear chain in the absence of entanglements, τ_e is the entanglement time, and $Z = N/N_e$ is the number of entanglements per chain, where N_e is the entanglement length. Measuring the strength of the flow in terms of Wi and the degree of entanglements in terms of Z allows a direct comparison with experimental result. Previous work on linear [24], ring [42], and ring-linear blends [43] shows excellent agreement between the experimentally observed extensional viscosity and simulation results using the model studied here. For the fully flexible model used here, $N_e \sim 84$ [44,45], $\tau_e = 10^4\tau$ [46], and we vary Wi from 0.1 to 32. All simulations were run using the Large Scale Atomic Molecular Massively Parallel Simulator (LAMMPS) [47] software.

The start-up extensional viscosities $\eta_E^+(\varepsilon)$ versus ε for $\mathrm{Wi} = 4$ for melts with interaction ratio α varying from 1 to 10 are plotted in Fig. 2(a). As α increases, our simulations capture the experimentally [10] observed transition from steady flow to solidlike yield and failure. For $\alpha \leq 4$, $\eta_E^+(\varepsilon)$ increases monotonically until approaching a plateau at large strain. For $\alpha = 6$, the startup viscosity increases nonmonotonically, exhibiting an overshoot around strain $\varepsilon \sim 2$ and reaches a steady state by $\varepsilon \sim 4$. As illustrated in Fig. 1, this change in behavior is associated with the heterogeneous breakup and flow of the system. For $\alpha \geq 8$, the stress maximum becomes more pronounced and is followed by a sudden drop in stress due to rapid strain localization and cavity formation. These cavitation events,

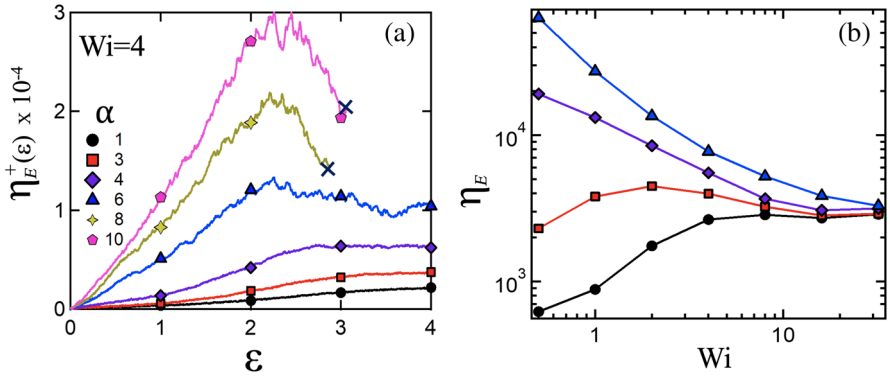

FIG. 2. (a) Transient extensional viscosity $\eta_E^+(\varepsilon)$ as a function of Hencky strain ε for association strengths $\alpha = 1, 3, 4, 6, 8$, and 10 at a $\mathrm{Wi} = 4$. A cross indicates the strain at which cavities are observed for $\alpha = 8$ and 10. (b) Terminal viscosities computed by averaging η_E over the strain interval from 5 to 10 versus Wi for $\alpha = 1$, 3, 4, and 6.

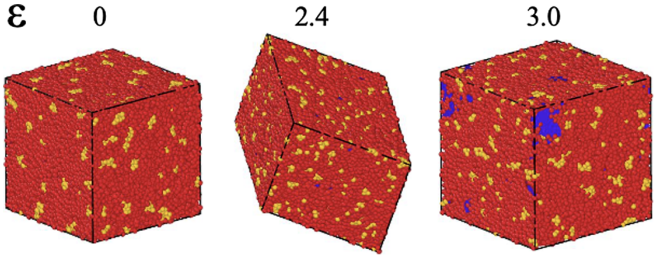

FIG. 3. Snapshots of systems with interaction ratio $\alpha = 10$ with cavities for Wi $= 4$ at strain $\varepsilon = 0$, 2.4 (maximum stress) and $\varepsilon = 3$. Nonassociating beads, stickers, and cavities are visualized by red, yellow, and blue colors, respectively.

shown in Fig. 3, are probably precursors to the runaway strain localization and macroscopic failure observed in filament stretching experiments [10].

The transition to solidlike yield, as the interaction ratio α increases, produces a massive rise in the terminal extensional viscosity, as shown in Fig. 2(b) for α from 1 to 6 and Wi from 0.5 to 32. At Wi $= 0.5$, η_E increases by 2 orders of magnitude as α increases from 1 to 6. Considering that only 5% of monomers are driving this large change in macroscopic dissipation, it is no wonder that these materials are so challenging to formulate and process. While all systems differ in dramatically in their dissipation at low Wi, they all approach a similar plateau in viscosity at high rates, Wi > 10. This convergence appears to be due to fragmentation of the clusters in sufficiently strong flows. In equilibrium, the average size of clusters increases significantly with increasing interaction ratio α [34], but we will show that strong extensional flow breaks up these clusters into smaller fragments. In nonassociating homopolymers, stress growth and steady-state dissipation are controlled by chain conformations elongating within the entanglement network. However, for these strongly associating systems, polymer elongation is instead mediated—or locally hindered—by chains coupling to a transient network of associating clusters. This produces enhanced strain hardening at all elongation rates, as shown in Fig. 4(a) which compares the stress-strain curves of $\alpha = 1$ and 6 systems for Wi from 0.5 to 32. Associating melts show large and roughly linear growth in stress with strain at all rates, while nonassociating melts exhibit much lower initial slopes and delayed strain hardening that only becomes appreciable above strains ~ 2.

The large stresses produced by elongating the chains drive the breakup of larger clusters of associating beads, reducing the average cluster size as shown in Fig. 4(b). A cluster's size is defined by the number of associating beads within 1.5σ of another member of the cluster. Similar results are obtained for cutoff distances of 1.4σ and 1.6σ. The average cluster size decreases gradually with increasing extensional stress and reaches a constant value for strains $\varepsilon \sim 3$. This cluster fragmentation process alters the temporary network and the coupling of chain

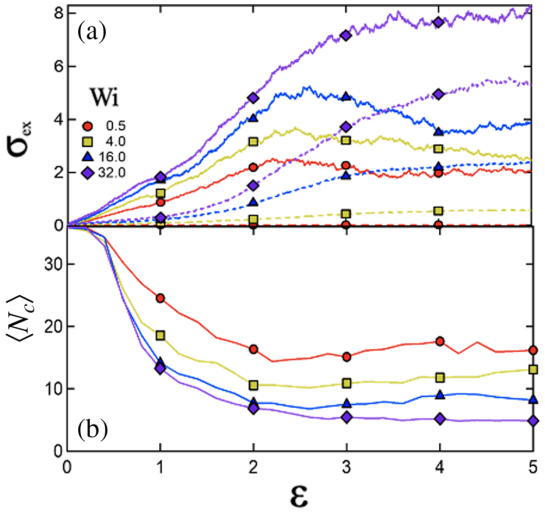

FIG. 4. (a) Extensional stress σ_{ex} for interaction ratio $\alpha = 1$ (dashed lines) and 6 (solid lines) and (b) average cluster size $\langle N_c \rangle$ as a function of strain ε for $\alpha = 6$ and Wi $= 0.5$, 4, 16, and 32.

conformations to the macroscopic flow, which can produce the heterogeneous behavior seen in Fig. 1.

The probabilities $P(N_c)$ of associating clusters of sizes N_c for $\alpha = 2$–6 are shown in Fig. 5 for equilibrium and for Wi $= 1$ and 8. The average $\langle N_c \rangle$ for all systems and Wi are shown in the inset of Fig. 5(c). In equilibrium, both $P(N_c)$ and the average cluster size N_c change significantly and qualitatively as the strength of the associating groups increases from $\alpha = 2$ to 6. At $\alpha = 2$, the most common cluster size is ~ 1 bead with a tail extending to larger sizes. As strength increases, $P(N_c)$ develops a well-defined peak of larger clusters. However, these differences diminish with increasing Wi as the flow breaks up larger clusters into smaller ones, producing distributions at low N_c that converge toward a common curve. Notably, for $\alpha = 6$, the system has no small clusters ($N_c < 10$) in equilibrium, but by Wi $= 8$, the flow-induced fragmentation process generates a distribution of small clusters that is qualitatively like the distributions of systems with weaker associations. At the highest Wi, $P(N_c)$ becomes independent of α as the flow becomes so strong that it overpowers the associative interactions. This coincides with the high-rate convergence of the terminal viscosity [Fig. 2(b)]. In this regime, advection drives the clusters to form and dissolve so rapidly that the viscosity becomes independent of the strength of the associating groups.

To capture these kinetics, the average contact lifetime of two associating beads was determined by measuring the time two associating groups remain continuously in contact. Here, two beads are in contact if separated by a distance less than 1.5σ. In equilibrium, for $\alpha > 3$ the average contact lifetime is immeasurably large (larger than the simulation time). However, under flow, the average lifetimes are significantly reduced as most associating groups stay in contact for very short times, less than 0.5τ,

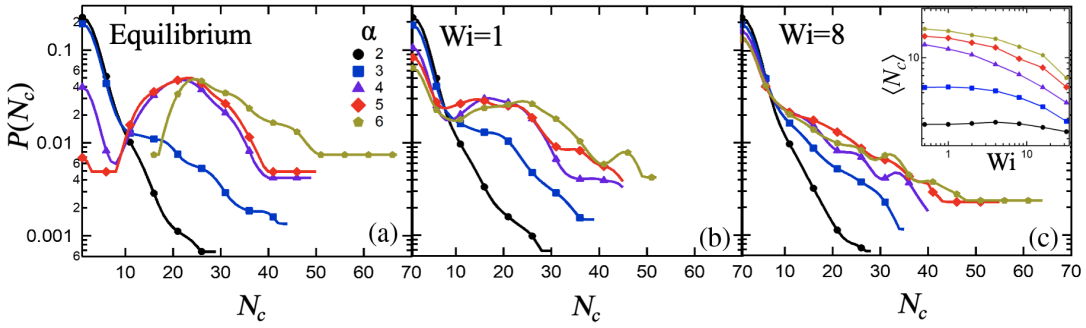

FIG. 5. Probability $P(N_c)$ as a function of cluster size N_c for interaction ratio $\alpha = 2$–6, (a) at equilibrium, (b) for Wi = 1, and (c) Wi = 8. The inset shows the average cluster size $\langle N_c \rangle$ as a function of Wi for corresponding systems.

before separating. This indicates that cluster fragmentation is dominated by advection, especially as cluster strengths increase. Interestingly, while fragmentation depends on mean cluster sizes, we find that the distribution of pairwise contact lifetimes becomes independent of Wi for large Wi.

The heterogeneous breakup of clusters drives a dynamic heterogeneity in the elongation of individual polymer chains. Figure 6 shows the probability distributions $P(R)$ of the end-to-end distances R of chains at several strains for Wi = 0.5, 4, and 32. For the nonassociating system ($\alpha = 1$), a narrow distribution at small R in equilibrium transitions to a narrow distribution at a large R by moving through a transient broad distribution. This intermediate broadening occurs because the susceptibility of individual chains to align in the flows depends upon their initial orientation and conformation, but eventually all the chains become elongated to a degree that increases with increasing Wi [24,25]. For strongly interacting associating groups ($\alpha = 6$), a fraction of chains stretch out, broadening the distribution, while other chains resist alignment because they are trapped within unyielding associating complexes. This produces a broad bimodal $P(R)$ as strain localizes and is accommodated by some chains that have been pulled taut enough to break free of anchoring points within large clusters.

The heterogeneous elongation of chains produces a self-reinforcing feedback with the cluster dynamics. As chains elongate toward full extension, they must maintain their backbone contour length, which inhibits the advection of larger clusters. This tends to reduce the size of clusters that elongated chains can participate in, which makes them even easier to elongate, further amplifying the effect. This feedback produces cross-correlations in $P(R)$ and $P(N_c)$. These results highlight that chain and cluster dynamics are

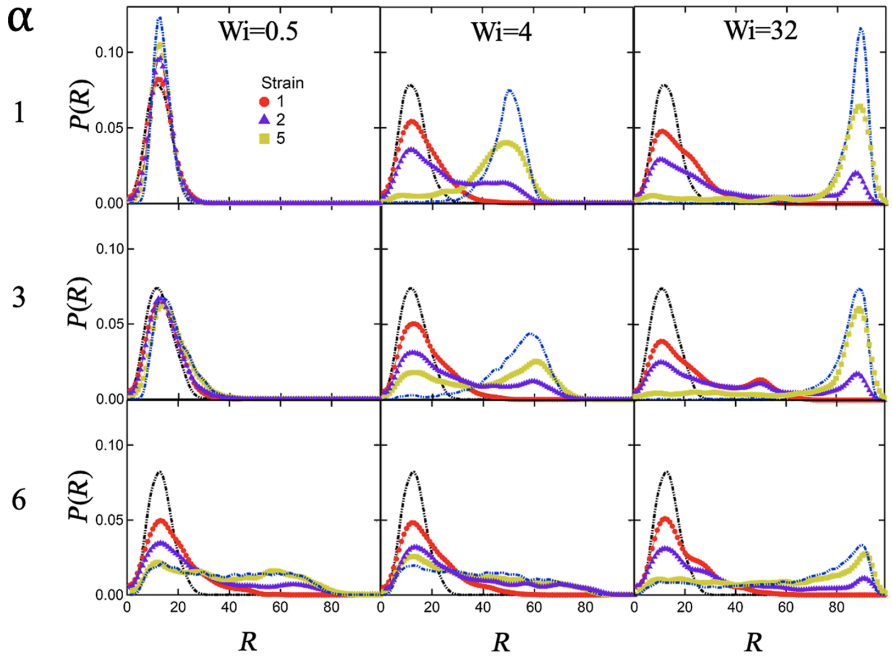

FIG. 6. Distribution function $P(R)$ of the end-to-end distance R for $\alpha = 1$, 3, and 6 for Wi = 0.5, 4, and 32 for strain $\varepsilon = 1$, 2, and 5. Black and blue dot-dashed lines correspond to $P(R)$ for equilibrium and average over strain interval 5–10, respectively.

highly correlated during nonlinear flow, and that these correlations can produce large changes in nanoscale structure and dynamics that can be used to engineer the nanoscale response of associating polymers to macroscopic deformations.

Our simulations have identified how a small fraction of associating groups along polymer backbones can dramatically alter the structure, dynamics, and deformation behavior of unentangled polymer melts. Increasing the association strength dramatically enhances both the extensional viscosity and strain hardening until systems eventually develop a yieldlike overshoot and fail by cavitation. For intermediate interaction strengths ~ 3–$6 k_B T$ and low rates, systems flow with an additional dissipation due to the work of breaking associations. As rates increase, chains develop a bimodal, stretching dynamics due to the heterogeneous breakup of associating clusters that localizes elongation in a fraction of the chains. Elongated chains hinder cluster convection and rapidly pull out of larger clusters, which makes it easier for them to elongate further.

In the limit of high strain rates, the viscous dissipation of all systems converges toward a common value independent of association strength α and strain rate. This appears to be due to the correlated dynamics of chain elongation and clusters fragmentation driving the cluster-size distribution $P(N_c)$ toward a system-independent distribution in strong flow.

Our results suggest that its unlikely experiments can get to a strain interval where there is a robust steady state as the dynamics are too slow relative to the strain limitations of experiments. However, these distributions can still be useful tools for understanding these highly correlated dynamics in transient flows. The approach of all systems toward a common limiting distribution at high rates provides a useful way point for rationalizing processing trends and constructing new theories. It also raises fundamental questions about whether similar behaviors occur during the elongation of other aggregating systems, such as physical gels. These correlations between cluster fragments, chain stretching, and elongational flow offer new insights into the rich mechanisms governing the rheology of a large class of soft matter systems.

D. P. gratefully acknowledges DOE Grant No. DE-SC007908. T. O. gratefully acknowledges startup funding provided by Carnegie Mellon University. The authors kindly acknowledge the use of computational resources provided by NSF No. MRI-1725573. This work was made possible in part by advanced computational resources deployed and maintained by Clemson Computing and Information Technology. This work was supported by the Sandia Laboratory Directed Research and Development Program. This work was performed, in part, at the Center for Integrated Nanotechnologies, an Office of Science User Facility operated for the U.S. Department of Energy (DOE) Office of Science. Sandia National Laboratories is a multimission laboratory managed and operated by National Technology & Engineering Solutions of Sandia, LLC, a wholly owned subsidiary of Honeywell International, Inc., for the U.S. DOE's National Nuclear Security Administration under Contract No. DENA-0003525. The views expressed in this article do not necessarily represent the views of the U.S. DOE or the U.S. Government.

[1] A. N. Beris, J. S. Horner, S. Jariwala, M. Armstrong, and N. J. Wagner, *Recent Advances in Blood Rheology: A Review*, Soft Matter **17**, 10591 (2021).
[2] D. B. Stein, G. De Canio, E. Lauga, M. J. Shelley, and R. E. Goldstein, *Swirling Instability of the Microtubule Cytoskeleton*, Phys. Rev. Lett. **126**, 028103 (2021).
[3] C. C. Hopkins, S. J. Haward, and A. Q. Shen, *Tristability in Viscoelastic Flow Past Side-by-Side Microcylinders*, Phys. Rev. Lett. **126**, 054501 (2021).
[4] G. de Souza and J. R. Tarpani, *Interleaving CFRP and GFRP with a Thermoplastic Ionomer: The Effect on Bending Properties*, Appl. Compos. Mater. **28**, 559 (2021).
[5] B. Li, C. Zhang, F. Peng, W. Wang, B. D. Vogt, and K. Tan, *4D Printed Shape Memory Metamaterial for Vibration Bandgap Switching and Active Elastic-Wave Guiding*, J. Mater. Chem. C **9**, 1164 (2021).
[6] W. Wang, J. Madsen, N. Genina, O. Hassager, A. L. Skov, and Q. Huang, *Toward a Design for Flowable and Extensible Ionomers: An Example of Diamine-Neutralized Entangled Poly (Styrene-co-4-Vinylbenzoic Acid) Ionomer Melts*, Macromolecules **54**, 2306 (2021).
[7] S. Seiffert *et al.*, *Supramolecular Polymer Networks and Gels* (Springer, Berlin, 2015), Vol. 268, p. 288.
[8] Z. Zhang, C. Huang, R. Weiss, and Q. Chen, *Association Energy in Strongly Associative Polymers*, J. Rheol. **61**, 1199 (2017).
[9] Z. Zhang, Q. Chen, and R. H. Colby, *Dynamics of Associative Polymers*, Soft Matter **14**, 2961 (2018).
[10] Z. R. Hinton and N. J. Alvarez, *The Trade-Off between Processability and Performance in Commercial Ionomers*, Rheol. Acta **58**, 499 (2019).
[11] Z. R. Hinton, A. Shabbir, and N. J. Alvarez, *Dynamics of Supramolecular Self-Healing Recovery in Extension*, Macromolecules **52**, 2231 (2019).
[12] J. N. Israelachvili, *Intermolecular and Surface Forces* (Academic Press, New York, 2015).
[13] S. Wu and Q. Chen, *Advances and New Opportunities in the Rheology of Physically and Chemically Reversible Polymers*, Macromolecules **55**, 567 (2022).
[14] A. Eisenberg, *Clustering of Ions in Organic Polymers. A Theoretical Approach*, Macromolecules **3**, 147 (1970).
[15] A. Shabbir, Q. Huang, Q. Chen, R. H. Colby, N. J. Alvarez, and O. Hassager, *Brittle Fracture in Associative Polymers: The Case of Ionomer Melts*, Soft Matter **12**, 7606 (2016).
[16] A. Shabbir, Q. Huang, G. P. Baeza, D. Vlassopoulos, Q. Chen, R. H. Colby, N. J. Alvarez, and O. Hassager, *Nonlinear Shear and Uniaxial Extensional Rheology of*

Polyether-Ester-Sulfonate Copolymer Ionomer Melts, J. Rheol. **61**, 1279 (2017).

[17] G. H. Ling, Y. Wang, and R. Weiss, *Linear Viscoelastic and Uniaxial Extensional Rheology of Alkali Metal Neutralized Sulfonated Oligostyrene Ionomer Melts*, Macromolecules **45**, 481 (2012).

[18] S. Wu, X. Cao, Z. Zhang, Q. Chen, Y. Matsumiya, and H. Watanabe, *Molecular Design of Highly Stretchable Ionomers*, Macromolecules **51**, 4735 (2018).

[19] S. L. Wingstrand, N. J. Alvarez, Q. Huang, and O. Hassager, *Linear and Nonlinear Universality in the Rheology of Polymer Melts and Solutions*, Phys. Rev. Lett. **115**, 078302 (2015).

[20] S. L. Morelly, L. Palmese, H. Watanabe, and N. J. Alvarez, *Effect of Finite Extensibility on Nonlinear Extensional Rheology of Polymer Melts*, Macromolecules **52**, 915 (2019).

[21] S. Costanzo, Q. Huang, G. Ianniruberto, G. Marrucci, O. Hassager, and D. Vlassopoulos, *Shear and Extensional Rheology of Polystyrene Melts and Solutions with the Same Number of Entanglements*, Macromolecules **49**, 3925 (2016).

[22] A. André, T. Shahid, F. Oosterlinck, C. Clasen, and E. Van *Ruymbeke, Investigating the Transition between Polymer Melts and Solutions in Nonlinear Elongational Flow*, Macromolecules **54**, 2797 (2021).

[23] T. Shahid, C. Clasen F. Oosterlinck, and E. van Ruymbeke, *Diluting Entangled Polymers Affects Transient Hardening but Not Their Steady Elongational Viscosity*, Macromolecules **52**, 2521 (2019).

[24] T. C. O'Connor, N. J. Alvarez, and M. O. Robbins, *Relating Chain Conformations to Extensional Stress in Entangled Polymer Melts*, Phys. Rev. Lett. **121**, 047801 (2018).

[25] T. C. O'Connor, A. Hopkins, and M. O. Robbins, *Stress Relaxation in Highly Oriented Melts of Entangled Polymers*, Macromolecules **52**, 8540 (2019).

[26] G. Ianniruberto and G. Marrucci, *Molecular Dynamics Reveals a Dramatic Drop of the Friction Coefficient in Fast Flows of Polymer Melts*, Macromolecules **53**, 2627 (2020).

[27] G. Ianniruberto, G. Marrucci, and Y. Masubuchi, *Melts of Linear Polymers in Fast Flows*, Macromolecules **53**, 5023 (2020).

[28] G. Ianniruberto, A. Brasiello, and G. Marrucci, *Simulations of Fast Shear Flows of PS Oligomers Confirm Monomeric Friction Reduction in Fast Elongational Flows of Monodisperse PS Melts as Indicated by Rheooptical Data*, Macromolecules **45**, 8058 (2012).

[29] T. Yaoita, T. Isaki, Y. Masubuchi, H. Watanabe, G. Ianniruberto, and G. Marrucci, *Primitive Chain Network Simulation of Elongational Flows of Entangled Linear Chains: Stretch/Orientation-Induced Reduction of Monomeric Friction*, Macromolecules **45**, 2773 (2012).

[30] C. Baig, V. G. Mavrantzas, and M. Kroger, *Flow Effects on Melt Structure and Entanglement Network of Linear Polymers: Results from a Nonequilibrium Molecular Dynamics Simulation Study of a Polyethylene Melt in Steady Shear*, Macromolecules **43**, 6886 (2010).

[31] C. McIlroy and P. D. Olmsted, *Deformation of an Amorphous Polymer during the Fused-Filament-Fabrication Method for Additive Manufacturing*, J. Rheol. **61**, 379 (2017).

[32] C. Schaefer, P. R. Laity, C. Holland, and T. C. McLeish, *Stretching of Bombyx mori Silk Protein in Flow*, Molecules **26**, 1663 (2021).

[33] C. Schaefer and T. C. B. McLeish, *Theoretical Rheo-Physics of Silk: Intermolecular Associations Reduce the Critical Specific Work for Flow-Induced Crystallisation*, arXiv:2112.01965.

[34] M. Senanayake, D. Perahia, and G. S. Grest, *Effects of Interaction Strength of Associating Groups on Linear and Star Polymer Dynamics*, J. Chem. Phys. **154**, 074903 (2021).

[35] K. Kremer and G. S. Grest, *Dynamics of Entangled Linear Polymer Melts: A Molecular-Dynamics Simulation*, J. Chem. Phys. **92**, 5057 (1990).

[36] R. Auhl, R. Everaers, G. S. Grest, K. Kremer, and S. J. Plimpton, *Equilibration of Long Chain Polymer Melts in Computer Simulations*, J. Chem. Phys. **119**, 12718 (2003).

[37] G. S. Grest, *Communication: Polymer Entanglement Dynamics: Role of Attractive Interactions*, J. Chem. Phys. **145**, 141101 (2016).

[38] P. J. Daivis and B. Todd, *A Simple, Direct Derivation and Proof of the Validity of the SLLOD Equations of Motion for Generalized Homogeneous Flows*, J. Chem. Phys. **124**, 194103 (2006).

[39] M. Dobson, *Periodic Boundary Conditions for Long-Time Nonequilibrium Molecular Dynamics Simulations of Incompressible Flows*, J. Chem. Phys. **141**, 184103 (2014).

[40] D. A. Nicholson and G. C. Rutledge, *Molecular Simulation of Flow-Enhanced Nucleation in N-Eicosane Melts under Steady Shear and Uniaxial Extension*, J. Chem. Phys. **145**, 244903 (2016).

[41] M. Doi and S. F. Edwards, *The Theory of Polymer Dynamics* (Oxford University Press, Oxford, 1988), Vol. 73.

[42] T. C. O'Connor, T. Ge, M. Rubinstein, and G. S. Grest, *Topological Linking Drives Anomalous Thickening of Ring Polymers in Weak Extensional Flows*, Phys. Rev. Lett. **124**, 027801 (2020).

[43] A. Borger *et al.*, *Threading–Unthreading Transition of Linear-Ring Polymer Blends in Extensional Flow*, ACS Macro Lett. **9**, 1452 (2020).

[44] S. K. Sukumaran, G. S. Grest, K. Kremer, and R. Everaers, *Identifying the Primitive Path Mesh in Entangled Polymer Liquids*, J. Polym. Sci. B Polym. Phys. **43**, 917 (2005).

[45] R. S. Hoy, K. Foteinopoulou, and M. Kröger, *Topological Analysis of Polymeric Melts: Chain-Length Effects and Fast-Converging Estimators for Entanglement Length*, Phys. Rev. E **80**, 031803 (2009).

[46] T. Ge, M. O. Robbins, D. Perahia, and G. S. Grest, *Healing of Polymer Interfaces: Interfacial Dynamics, Entanglements, and Strength*, Phys. Rev. E **90**, 012602 (2014).

[47] A. P. Thompson *et al.*, LAMMPS—*A Flexible Simulation Tool for Particle-Based Materials Modeling at the Atomic, Meso, and Continuum Scales*, Comput. Phys. Commun. **271**, 108171 (2022).